Modulation Resonance Enhancement in SCH Quantum-Well Lasers with an External Bragg Reflector

Malin Premaratne, *Student Member, IEEE,* and Arthur J. Lowery, *Senior Member, IEEE*

***Abstract*— The modulation response of a semiconductor laser can be enhanced by coupling it to an external cavity with frequency-selective feedback. This creates a comb of transmission bands where the modulation response is high, at the cavity round-trip frequency and its harmonics. In a previous publication, we related the bandwidths of these bands to the material and structural parameters of a bulk laser. We showed that a nonzero linewidth enhancement factor together with a nonzero intermediate facet reflectivity lead to deep nulls close to the peaks of these transmission bands. This suggests that quantum-well (QW) lasers, which have a low linewidth enhancement factor, may give a better performance than bulk lasers. To test this hypothesis, we have extended our analysis to model QW lasers coupled to a fiber grating. Carrier transport, carrier heating, intraband carrier fluctuations, and nonparabolic band structures are considered. We show that electron carrier transport and amplitude-phase coupling in the separate-confinment-heterostructure (SCH) layer contribute to the nulls in the modulation response. Therefore, the apparent advantage of having a reduced linewidth enhancement factor that we found in our previous analysis cannot be fully realized by using QW lasers.**

***Index Terms*— External cavity, fiber Bragg grating, modeling modulation, resonance enhancement, SCH quantum-well lasers.**

I. Introduction

FIBER-OPTIC links could replace waveguides and coaxial cables for conveying millimeter waves in applications such as antenna feeds, phase array radars [1], [2], and subcarrier multiplexed systems [3]–[5]. The development of optical fiber links with low loss, low cost, low dispersion, and high dynamic range has much to do with this success [2]. In addition, the immunity to electromagnetic interference of optical fiber links reduces crosstalk and thus allows systems with higher component densities [2], [4], [5]. However, noise, nonlinearities [6], and bandwidth constraints [7], [8] of the optical source affect signal quality. Fortunately, the modulation response of a semiconductor laser can be enhanced by coupling an external cavity [7], [9] with strong feedback. This creates resonantly enhanced transmission windows close to the cavity round-trip frequency and its harmonics [3], [4], [7], [9].

Manuscript received May 19, 1997; revised November 24, 1997. This work was supported in part by the Australian Photonics Cooperative Research Centre, the Photonics Research Laboratory, the University of Melbourne, and by the Grace Matthaei Scholarship Committee.

The authors are with the Australian Photonics Cooperative Research Centre, Photonics Research Laboratory, Department of Electrical and Electronic Engineering, The University of Melbourne, Parkville, Vic. 3052, Australia.

Publisher Item Identifier S 0018-9197(98)02390-2.

In 1982, Sullivan *et al.* [10] proposed fiber grating external cavity lasers as a means of improving the performance of solitary Fabry–Perot laser diodes. A detailed experimental investigation of their proposal was carried out by Hammer *et al.* [11]. They demonstrated that fiber grating external cavity lasers could maintain single-mode operation over a wide range of injection currents and temperatures. However, due to a reduction of the small-signal bandwidth as a result of the increase in photon lifetime due to the external cavity, these lasers were not considered useful as directly modulated transmitters. Therefore, until recently, fiber grating external cavity lasers found use only in mode locking [12] and CW tunable source applications. However, resonantly enhanced modulation is useful for narrow-band millimeter-wave transmission systems [3], [4], [7]. These schemes find difficulties in practice due to the resonance enhancement of noise and the appearance of nulls close to the resonance peak [9], [13]. In a previous publication [9], we modeled a resonantly enhanced external-cavity laser and analyzed the noise and the appearance of nulls close to resonance peaks. However, our analysis was limited to bulk lasers [14].

In this paper, a detailed analysis of a fiber-grating reflector strong-feedback external-cavity laser [15] with a quantum-well (QW) active layer [16]–[18] is presented. Although there have been many studies on bulk lasers with strong feedback from an external cavity [9], [13], [19]–[22], this paper presents the first detailed study on a QW laser coupled to an external cavity with strong feedback. The carrier transport [23], [24] has been included and predicts a reduction in relaxation resonance frequency [25] and an increase in the parasitic-like roll-off in the modulation response [25]. In addition to similar effects observed in bulk lasers with externally coupled resonators [9], we show that there is a reduction in the bandwidth of the resonance peaks due to the electron carrier transport time and amplitude-phase coupling in the separate-confinement-heterostructure (SCH) layer. In [9], we showed that a low linewidth enhancement factor leads to an improved modulation response due to the suppression of nulls appearing close to resonance peaks and hence widening the transmission windows bandwidths. Therefore, external-cavity lasers with QW active layers were expected to give superior bandwidths due to an inherently low linewidth enhancement factor and thus suppressed amplitude-phase coupling effects. However, here we show that carrier injection, carrier confinement, and carrier transport associated with material and geometrical

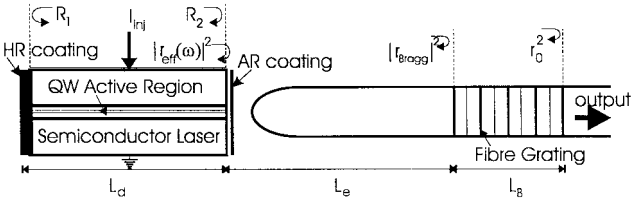

Fig. 1. Fiber grating external cavity laser. (AR: antireflection coating; HR: high reflective coating).

structural parameters may degrade the performance in these devices by:

1) decreasing transmission window bandwidth due to nulls close to the cavity resonance-peaks;
2) decreasing the modulation efficiency due to the usual parasitic-like role-off of multiple-quantum-well (MQW) structures with a SCH region (due to carrier transport effects).

We also show that carrier escape times from the QW decrease the modulation efficiency at high frequencies. A signal flow graph for the QW active layer with strong external feedback is drawn and is compared with a signal flow graph of a bulk laser with a similar architecture [9]. We use these signal flow graphs to explain the physics behind the observed small signal behavior.

This paper is organized as follows. In Section II, we present the detailed theoretical modeling of fiber-grating external-cavity lasers with a QW active gain medium, including intraband relaxations, carrier transport, carrier heating, and nonparabolic band effects. In Section III, we use this model to analyze the modulation efficiency, and compare our results with those for bulk lasers of similar architecture. In Section IV, we discuss the mechanism behind these results. Section V will summarize the results and concludes this paper.

II. Analytical Model

Fig. 1 shows the device under consideration. It consists of a Fabry–Perot (FP) laser diode with high-reflectivity (HR) and antireflection (AR) coated facets. The light from the AR-coated facet is coupled to the fiber Bragg grating reflector. The output power is taken through the grating. The grating reflectivity is kept reasonably low (i.e., Bragg grating coupling strength ≤ 1) to ensure a reasonably high output power [26].

Fig. 2 shows the schematic diagram of the model used in a QW active layer. The quantum confinement has been achieved by sandwiching an $In_{1-x}Ga_xAs$ layer between two $In_{1-x}Ga_xAs_yP_{1-y}$ barrier layers lattice matched to InP [27], [28]. As the experimental studies on external cavity lasers with strong frequency-selective feedback suggest that they operate predominantly in transverse electrical (TE) mode [11], [15], [20], the GaAs mole fraction in $In_{1-x}Ga_xAs$ is assumed to be less than 0.48 to introduce compressive strain into the QW region [27]. This enables the QW to have a high TE gain compared with the TM gain. The well width was adjusted in our model to allow the maximum gain to be within the 1.55-μm telecommunications window. As we concentrate mainly on frequencies greater than carrier

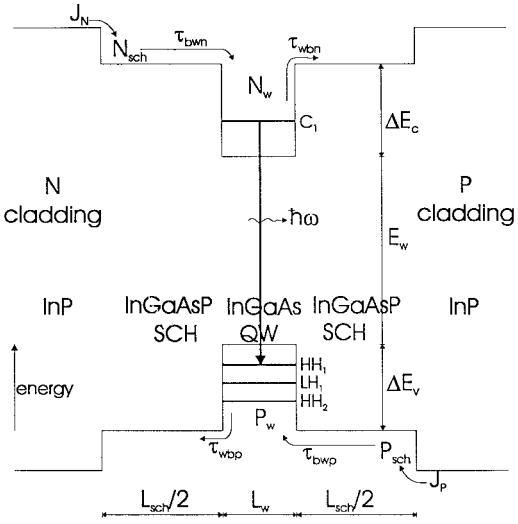

Fig. 2. Band diagram of the QW active layer. The QW is formed by sandwiching a $In_{1-x}Ga_xAs$ between $In_{1-x}Ga_xAs_yP_{1-y}$ layers lattice matched to InP cladding layers.

thermonic emission rate from the QW, we do not use the ambipolar approximation and so treat the electrons and holes separately [29]. At these frequencies, the intraband dynamics [30] also become important [31], [32]. Therefore, we use non-Fermian distributions and carrier temperature fluctuations in our model [33]. This enables us to include both spectral hole burning and carrier heating effects [32]. The gain is modeled by solving the Luttinger–Kohn Hamiltonian [34], taking strain into account using the Pikus–Bir Hamiltonian [35]. In the calculations of subband energy dispersion, we limit ourselves to the 4×4 Pikus–Bir Hamiltonian [35] for the valence band and the parabolic band approximation for the conduction band [36]. The density matrix formalism [37], [38] is used to calculate gain, and differential-gain-related parameters such as refractive index fluctuations and the linewidth enhancement factor [39], [40].

The linear and nonlinear effects resulting from carrier–photon interaction are modeled using an extended multiple reflection, strong feedback model given by Park *et al.* [41] Following the treatment of Rong-Qing *et al.* [42], multiple reflections were handled compactly using an assumption of stationarity (i.e., independent of time reference) of the field components. The validity of this stationarity argument can be justified by noting that our analysis is restricted to periodic and steady-state conditions. However, the treatment of Rong-Qing *et al.* [42] failed to recognize the importance of delayed laser amplitude and phase components after multiple reflections and these were replaced with first-order differentials. By retaining the delayed laser field amplitudes and phases after multiple reflections, we extend our analysis to comparatively longer cavities and also retain the delay-induced interference effects, which we have shown [9] to be critical in predicting peaks and nulls in the noise and modulation spectra.

A. Carrier–Photon Interaction Model

Experimental studies with strong-feedback external-cavity lasers have shown that they could maintain strong stable

TABLE I
EXTERNAL CAVITY LASER PARAMETERS

Parameter	Description	Value	Units
c	speed of light in vacuum	3.0×10^{8}	m·s^{-1}
q	electron charge	1.602×10^{-19}	C
h	Planck's constant	6.626×10^{-34}	J·K^{-1}
k	Boltzmann's constant	1.381×10^{-23}	J·K^{-1}
L	solitary laser diode length	300.0	μm
D	solitary laser diode depth	0.2	μm
L_e	external cavity length	†, ‡	m
L_B	fiber Bragg grating length	8.0	mm
Λ_B	Bragg grating period	516.33	nm
κL_B	coupling strength of grating	1.0	
$n_{B,0}$	effective index of the fiber	1.5	
n_e	effective index	3.4	
n_g	group index	3.4	
C	feedback coupling efficiency	1.0	
V_g	group velocity in laser medium	8.824×10^{7}	m·s^{-1}
α_H	linewidth enhancement factor	†	
χ	phase variation constant in the SCH region	2.0, †	
α_L	scattering loss	3000.0	m^{-1}
α_B	grating power-loss coefficient	0.0	m^{-1}
Γ	field confinement factor	$1.67\times10^{6}\,L_w$	
R_1	reflectivity of HR coated facet	0.9025	
R_2	intermediate facet reflectivity	1.0×10^{-4}	
r_0^2	grating interface reflectivity	0.0	
β	spontaneous emission coupling factor	1.0×10^{-4}	
$I_{\rm inj}$	injection current	†	mA
τ	external cavity round-trip time	†, ‡	s
τ_L	solitary laser round-trip time	†, ‡	s
$\overline{\omega}$	angular frequency (without feedback)	‡	rad/s
ω	angular frequency (with feedback)	‡	rad/s
τ_{spp}	Shockley–Read–Hall coefficient (holes)	5.0×10^{-10}	s
τ_{spn}	Shockley–Read–Hall coefficient (electrons)	5.0×10^{-10}	s
B	bimolecular recombination coefficient	8.0×10^{-17}	m^{6}·s^{-s}
C_p	Auger recombination coefficient (holes)	7.5×10^{-41}	m^{9}·s^{-1}
C_n	Auger recombination coefficient (electrons)	7.5×10^{-41}	m^{9}·s^{-1}
τ_{hwp}	carrier transport time (holes)	50.0, †	ps
τ_{hwn}	carrier transport time (electrons)	1.0, †	ps
τ_{wbp}	well-barrier escape time (holes)	1.0, †	ns
τ_{wbn}	well-barrier escape time (electrons)	50.0, †	ps
τ_{hv}	carrier phonon collision time (holes)	1.0	ps
τ_{hc}	carrier phonon collision time (electrons)	1.0	ps
τ_{hv}	hole dephasing time	0.1	ps
τ_{hv}	electrons dephasing time	0.1	ps

† These quantities are varied in calculations and given in text and in figure captions.
‡ These quantities are calculated using details given in text.
†, ‡ In this instance, it depends on the context.

single-mode operation, even under high-power operation [12], [43], [44]. The reason for strong, stable single-mode operation is easily justified for external mirrors having bandwidths narrower than the external-cavity mode spacing. However, Doerr *et al.* [45] have recently shown that these results hold even for lasers with an external mirror having a bandwidth of a few external cavity modes. They showed that intermodulation between adjacent modes transfers power between the modes, leading to a central, dominant mode. Recently we showed that experimental observations of a strong feedback external-cavity laser can be reproduced in detail using a single-mode model with intrinsic nonlinearities of the lasing process [9]. However, we believe that the actual mechanism responsible for this experimentally observed strong single-mode operation needs to be further studied in detail before any conclusion can be reached. Considering these reasons, we limit our study to the single-mode case, as it is sufficient to account for significant experimental observations [9], [44].

By design, the active layer volume is at least one order of magnitude smaller than the SCH volume [46]. Therefore, a significant proportion of the optical mode is confined outside the active layer and guided by the SCH. Hence, the optical phase of the guided lasing mode is affected by the index changes in both active and SCH layers. As the index variations in active and SCH layers depend on the respective carrier concentrations, we can write the effective index variation $n_{\rm eff}$ seen by the lasing mode with respect to QW electron density N_w as [47]

$$\frac{\partial n_{\rm eff}}{\partial N_w} = \Gamma\frac{\partial n_{\rm effw}}{\partial N_w} + (1-\Gamma)\frac{\partial n_{\rm effb}}{\partial N_b}\frac{\partial N_b}{\partial N_w} \tag{1}$$

where the variables used are defined in Table I. If we consider the phase change associated with the refractive index variation, and trace multiple passes of optical field through the active region and external cavity, then the following equations characterize the temporal evolution of the intensity I and phase φ:

$$\begin{aligned}\frac{dI}{dt} &= [\Gamma G - \alpha_L + \ln(R_1R_2)/\tau_L]I \\ &\quad + 2\{\mathrm{Re}[\ln(f)]/\tau_L\}I + \Gamma\beta BN_wP_w \end{aligned}\tag{2}$$

$$\begin{aligned}\frac{d\varphi}{dt} &= (\varpi-\omega_s) + 0.5\Gamma\alpha_{gsp}[G-\alpha_L+\ln(R_1|R_{\rm eff}|)/\tau_L] \\ &\quad + (1-\Gamma)\chi\Delta N_b + \mathrm{Im}[\ln(f)]/\tau_L \end{aligned}\tag{3}$$

where $\Gamma G = \Gamma G(\omega_s, N_w, P_w, I, T_e, T_h)$ is the modal gain of the active layer. The definitions of the other parameters are given in Table I. These equations are different to the equations used by Park *et al.* [41] and Premaratne *et al.* [9] due to the inclusion of phase dynamics using (1) and the nonlinear gain introduced later. In (2) and (3), the external cavity effects were included by incorporating a lumped parameter f. Considering multipass reflections in the external cavity, f can be written as [41], [42]

$$\begin{aligned}f(\omega) &= 1 + \hat{C}\frac{r_{\rm Bragg}}{\sqrt{R_2}}(1-R_2) \\ &\quad\cdot\sum_{n=1}^{\infty}\sqrt{\frac{I(t-n\tau)}{I(t)}}\left(-\sqrt{R_2}\,r_{\rm Bragg}\right)^{n-1} \\ &\quad\cdot\exp\{-j\omega n\tau + j[\varphi(t-n\tau)-\varphi(t)]\}\end{aligned}\tag{4}$$

where $r_{\rm Bragg}$ is the field reflection coefficient of the Bragg grating. Assuming the effective index variation along the fiber

grating from an unperturbed index n_{BO} with amplitude index perturbation Δn_B is [48]

$$n_B(z) = n_{BO} + \Delta n_B \cos\left(\frac{2\pi}{\Lambda_B} z + \vartheta_B\right) \tag{5}$$

and writing the coupled mode equations [49] for forward and backward traveling wave envelopes E^+ and E^- as

$$\frac{dE^+}{dz} = -\left(\frac{\alpha_B}{2} + j\delta\right) E^+ - j\kappa e^{-j\vartheta} E^- \tag{6}$$

$$\frac{dE^-}{dz} = \left(\frac{\alpha_B}{2} + j\delta\right) E^- + j\kappa e^{j\vartheta} E^+ \tag{7}$$

we can calculate the field reflectivity of Bragg grating $r_{\text{Bragg}} = (E^+/E^-)_{Z=0}$ as (8) [48], shown at the bottom of the page, where $\delta = (\omega n_{BO}/c - \pi/\Lambda_B)$ is the detuning of the lasing frequency from Bragg condition, $\beta_B = \pi/\Lambda_B$, $\gamma_B^2 = (\alpha_B/2 + j\delta)^2 + \kappa^2$, and r_0^2 is the reflectivity of the grating to fiber coupling interface as shown in Fig. 1. Noting that r_{Bragg} is a complex quantity, it can be written in polar form, $r_{\text{Bragg}} = |r_{\text{Bragg}}| \exp(j\angle r_{\text{Bragg}})$. The magnitude $|r_{\text{Bragg}}|$ gives the lasing frequency-dependent reflectivity while the phase $\angle r_{\text{Bragg}}$ induces a lasing frequency-dependent delay [i.e., delay $= \partial/\partial\omega(\angle r_{\text{Bragg}})$] to the reflected field. This leads to the change of effective cavity length with lasing frequency and hence a change in the cavity's modulation resonance frequency. This effective length variation of the external cavity and the SCH and QW carrier-density-dependent variation of the solitary laser effective cavity length have been taken into account in the present analysis for accurate interpretation of results.

Though a simple logarithmic gain model [50] with gain suppression is sufficient to explain most characteristics of the composite lasing system, a detailed nonlinear gain model is desirable as it includes carrier heating, lattice strain, energy band nonparabolic effects, and intraband relaxation effects. Even more, some of the parameters used in our model have not been measured experimentally. Therefore, a detailed gain model is desired for calculating these parameters from the known values of fundamental parameters. Conventionally, many of the stimulated emission related effects were modeled assuming a parabolic profile for the conduction and valence bands [51]. This parabolic band assumption has enabled the researchers to develop a gain model having a logarithmic carrier density dependency [55]. It is interesting to note that due to its simplicity, the logarithmic gain model fails to account for carrier temperature fluctuations and electron–hole interactions in the semiconductor lattice [32]. Furthermore, recent studies have shown that a simple parabolic assumption for valence bands is not adequate due to the interband coupling among heavy hole, light hole, and spin split-off bands [36], [52]. Recent advances in the epitaxial growth technologies have shown that intentionally introduced strain or stress could significantly change the valence band profile [53]. Furthermore, it has been shown in literature that by appropriately controlling the lattice mismatch, isotropic (hydrostatic) and anisotropic (shear) strain, the polarization dependence of the gain (i.e., TE, TM sensitivity) could be enhanced or suppressed [46], [53]. Therefore, an adequate representation of the lattice mismatch introduced strain effects is a must for a realistic gain model.

Using the multiband effective mass theory with an envelope function approximation, we can calculate the heavy and light hole band structure by solving the following set of equations [54]:

$$\sum_{v'} [H_{vv'} + V(z)\delta_{vv'}] g_m^{v'}(k_{||}, z) = E_m(k_{||}) g_m^v(k_{||}, z), \quad v, v' \in \{1, 2, 3, 4\} \tag{9}$$

where $k_{||} = (k_x, k_y)$ is the in-plane wave vector, $E_m(k_{||})$ is the subband energy for the valence band, $V(z)$ is the potential profile in the valence band and $g_m^v(k_{||}, z)$ are the envelope functions. The elements of the 4×4 Pikus–Bir Hamiltonian [35], $H_{vv'}$ is calculated using the $\boldsymbol{k}\cdot\boldsymbol{p}$ method [36], [52], [54]

$$H_{vv'} = \begin{pmatrix} P+Q & -S & R & 0 \\ -S^+ & P-Q & 0 & R \\ R^+ & 0 & P-Q & S \\ 0 & R^+ & S^+ & P+Q \end{pmatrix} \tag{10}$$

where the parameters P, Q, R, and S are given using Luttinger parameters [36], [52] as

$$P = \frac{\hbar^2}{2m_0}\gamma_1\left(k_x^2 + k_y^2 - \frac{\partial^2}{\partial z^2}\right) - 2a\left(\frac{C_{11} - C_{12}}{C_{11}}\right) \cdot \left[1 - \frac{a(x)}{a_0}\right] \tag{11.1}$$

$$Q = \frac{\hbar^2}{2m_0}\gamma_2\left(k_x^2 + k_y^2 + 2\frac{\partial^2}{\partial z^2}\right) - b\left(\frac{C_{11} + 2C_{12}}{C_{11}}\right) \cdot \left[1 - \frac{a(x)}{a_0}\right] \tag{11.2}$$

$$R = \frac{\hbar^2}{2m_0} 2\sqrt{3}[\gamma_2(k_x^2 - k_y^2) - 2j\gamma_3 k_x k_y]$$

$$R^+ = \frac{\hbar^2}{2m_0} 2\sqrt{3}[\gamma_2(k_x^2 - k_y^2) + 2j\gamma_3 k_x k_y] \tag{11.3}$$

$$S = -j\frac{\hbar^2}{2m_0} 2\sqrt{3}\gamma_3(k_x - jk_y)\frac{\partial}{\partial z}$$

$$S^+ = -j\frac{\hbar^2}{2m_0} 2\sqrt{3}\gamma_3(k_x + jk_y)\frac{\partial}{\partial z}. \tag{11.4}$$

The definitions and values of the parameters used in the above expressions are given in Table II. Due to weak interac-

$$r_{\text{Bragg}} = \frac{r_0 \exp[-j(2\beta_B L_B + \vartheta_B)]\,[\gamma_B \cosh(\gamma_B L_B) - (\alpha_B/2 + j\delta)\sinh(\gamma_B L_B)] - j\kappa \sinh(\gamma_B L_B)}{\gamma_B \cosh(\gamma_B L_B) + \{(\alpha_B/2 + j\delta) + j\kappa r_0 \exp[-j(2\beta_B L_B + \vartheta_B)]\}\sinh(\gamma_B L_B)} \tag{8}$$

TABLE II
QW MATERIAL $In_{1-x}Ga_xAs$

Parameter	Description	Value	Units
x	GaAs mole fraction	0.41	
L_w	quantum well width	7.0	nm
V_w	volume of the QW region =(LDL_w)	4.2×10^{-19}	m^3
$a(x)$	$In_{1-x}Ga_xAs$ lattice constant	6.0584-0.4051x	A^0
E_w	band gap energy	0.324+07x+0.4x^2	eV
Δ	spin-orbit-split-off energy	0.38-0.04x	eV
γ_1	1st Luttinger parameter	20.4-13.55x	
γ_2	2nd Luttinger parameter	8.3-6.2x	
γ_3	3rd Luttinger parameter	9.1-6.2x	
C_{11}	stiffness constant	(8.329+3.551x) $\times10^{11}$	dyn/cm^2
C_{12}	stiffness constant	(4.526+0.854x) $\times10^{11}$	dyn/cm^2
a	hydrostatic deformation potential	-6-3.71x	eV
b	strain deformation potential	-1.8+0.1x	eV

tion between conduction and valence band levels, we used a parabolic band approximation to calculate the corresponding conduction band energy levels. This restriction can easily be modified by using 8×8 Pikus–Bir Hamiltonian [35]. However, no significant improvement in qualitative or numerical description is introduced due to this. The 4×4 Pikus–Bir Hamiltonian [35] gives a much improved gain model compared with the conventional logarithmic gain model (see [36] and [54] for details). This is due to the fact that the logarithmic gain model can be derived by ignoring light hole bands and assuming a parabolic profile for the energy bands [55]. Therefore, logarithmic gain models fail to take strain effects explicitly [55] and also have a restricted parameter space due to the increased use of fitted parameters. As we treat electrons and holes separately and incorporate carrier heating effects into our analysis, this detailed model gives the required parameter space for the calculation of intermediate quantities used in the small-signal analysis.

Using the above calculated energy bands for conduction and valence bands, and using density matrix theory, we can write the following expression for the nonlinear TE gain [32]:

$$G(\omega, N_w, P_w, T_e, T_h) = \frac{q^2\pi}{n_e c\varepsilon_0 m_0^2\omega}\sum_{m,n}\int |\mu_{m,n}|^2 \cdot \frac{[f_m^c(k_t)-f_n^v(k_t)]\,(\gamma/\pi)}{(E_{mn}^{cv}-\hbar\omega)^2+\gamma^2+\gamma|\mu_{m,n}|^2\dfrac{\omega(\tau_e+\tau_h)}{\varepsilon_0 n_e^2}I}\frac{k_t dk_t}{2\pi L_w} \tag{12}$$

where $|\mu_{m,n}|^2$ [51], [52] is the momentum element of the polarization vector for the transition from the mth conduction band to the nth valence band and E_{mn}^{cv} is the corresponding transition energy associated with the above two levels. The Fermi functions [32] of electron and hole occupation probabilities is given for electron temperature T_e and hole temperature T_h as

$$f_m^c(k_t) = \frac{1}{1+\exp\left[\dfrac{E_m^c(k_t)-F_c}{k_B T_e}\right]} \tag{13.1}$$

$$f_n^v(k_t) = \frac{1}{1+\exp\left[\dfrac{E_n^v(k_t)-F_v}{k_B T_h}\right]} \tag{13.2}$$

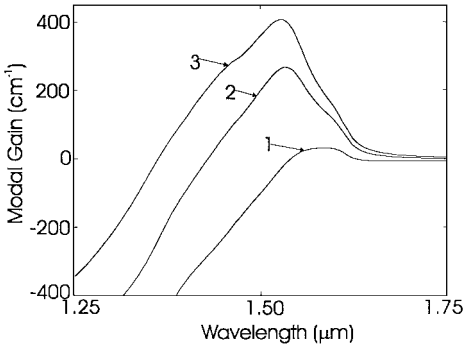

Fig. 3. Modal gain spectrum for active layer considered in this paper for carrier densities of 1.0×10^{24} m^{-3}, 2.0×10^{24} m^{-3}, and 3.0×10^{24} m^{-3}.

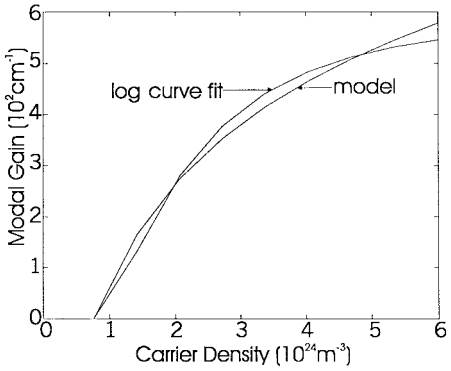

Fig. 4. Peak gain (modal) against active layer carrier density. For comparison, a least-square fit of the commonly used $g_0\ln(N/N_0)$ is also given. (N: carrier density), $g_0 = 2.8492\times10^2$ cm^{-1} and $N_0 = 0.789\,45\times10^{24}$ m^{-3}.

where F_c and F_v are the quasi-Fermi levels of electrons and holes [36], [54], [55]. The carrier temperature effects are introduced to the gain model through these Fermi functions. As these relations are inherently nonlinear, carrier temperature fluctuations lead to the introduction of carrier heating related gain suppression terms into the QW gain. Fig. 3 shows the gain spectra calculated using (12) for GaAs mole fraction $x = 0.41$. The gain spectra used in the model are calculated by fitting polynomial fractions around these curves close to operating points. These calculations were made using a MATLAB package equipped with the SPLINE Toolbox software. Fig. 4 shows the peak gain against the active region carrier density. For comparison, the often used $g_0\ln(N/N_0)$ model is also plotted there. A mean square curve-fitting algorithm was used to find g_0 and N_0. This figure shows that the logarithmic gain model gives a fairly accurate representation of the more detailed model. However, the major drawback of this logarithmic model results due to its inability to give an explicit parametric dependency of g_0 and N_0 with the more fundamental device parameters. Formulations similar to (12) were used to calculate the refractive index change in the active region, the linewidth enhancement factor, the nonlinear gain coefficients for spectral hole burning, and carrier heating effects. Fig. 5 shows that the linewidth enhancement factor is dependent on the carrier density. However, the linewidth enhancement remains low even for high carrier densities, compared with that in bulk lasers.

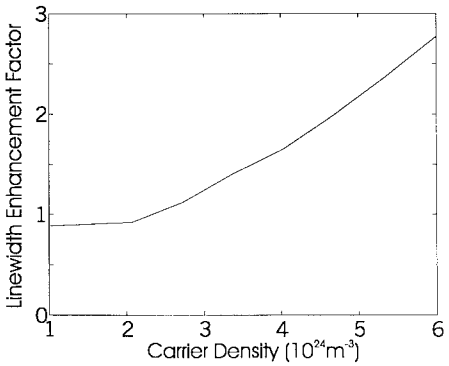

Fig. 5. Linewidth enhancement factor against active layer carrier density.

B. Carrier Injection Model

The presence and the time scales of carrier transport and carrier capture/emission have been shown to significantly influence the direct modulation response of the QW lasers [46], [47] by reducing the relaxation resonance frequency and increasing the parasitic-like role-off in the modulation response of solitary QW lasers [46], [47]. Additionally, these processes reduce the effective differential gain and increase the effective linewidth enhancement factor [46]. However, all these studies were for solitary lasers without any feedback effects. Therefore, the question remains whether the carrier transport and related effects are important in resonantly enhanced QW lasers.

We assume that the QW and SCH carriers can be separated into four discrete levels, representing electron and hole concentrations separately [29]. These electrons and holes diffuse and drift toward each other due to carrier gradients and mutual interactions. In the case of a graded index (GRIN) SCH QW laser [56], the built-in electric field in the GRIN layer aids this process. The separate treatment of electron and hole concentrations in QW and SCH layers allows us to exclude the ambipolar approximation from the model [29]. This leads to much improved description of the device at high frequencies due to the consideration of finite dielectric relaxation times [29]. This can be explained by noting that for modulation frequencies higher than $1/(2\pi\tau_{wbn})$ (which normally exceed the dielectric relaxation time), violation of charge neutrality results due to the trapping of electrons in the QW [29]. Therefore, it becomes essential to treat electrons and holes separately for accurate prediction of the millimeter-wave modulation performance. This has been demonstrated by Suzuki *et al.* [29] for solitary QW lasers by comparing with experimental results. Modifying the rate-equation model given in [29] by including the nonlinear gain model developed earlier and introducing Shockley–Read–Hall, bimolecular, and Auger recombination processes, we get the following set of equations with carrier capture, escape, and transport effects:

$$\frac{dN_b}{dt} = J_N - \frac{N_b}{\tau_{bwn}} + \frac{V_w}{V_b}\frac{N_w}{\tau_{wbn}} \tag{14}$$

$$\frac{dP_b}{dt} = J_P - \frac{P_b}{\tau_{bwp}} + \frac{V_w}{V_b}\frac{P_w}{\tau_{wbp}} \tag{15}$$

$$\frac{dN_w}{dt} = \frac{V_b}{V_w}\frac{N_b}{\tau_{bwn}} - \frac{N_w}{\tau_{wbn}} - GI - \frac{N_w P_w}{\tau_{spn}P_w + \tau_{spp}N_w} - BN_wP_w - C_N N_w^2 P_w - C_P N_w P_w^2 \tag{16}$$

TABLE III
SCH MATERIAL $In_{1-x}Ga_xAs_yP_{1-y}$ LATTICE MATCHED TO InP: $x = 0.1894y/(0.4184 - 0.013y)$

L_b	SCH region width	70.0	nm
V_b	volume of the SCH region=(LDL_b)	4.2×10^{-18}	m^3
E_b	band gap energy	0.96	eV
γ_1	1st Luttinger parameter	4.95+15.45y-0.9x-12.65xy	
γ_2	2nd Luttinger parameter	1.65+6.65y-1.16x-5.04xy	
γ_3	3rd Luttinger parameter	2.35+6.75y-1.1x-5.1xy	
a_0	InP lattice constant	5.8688	A^0

$$\frac{dP_w}{dt} = \frac{V_b}{V_w}\frac{P_b}{\tau_{bwp}} - \frac{P_w}{\tau_{wbp}} - GI - \frac{N_w P_w}{\tau_{spn}P_w + \tau_{spp}N_w} - BN_wP_w - C_N N_w^2 P_w - C_P N_w P_w^2 \tag{17}$$

where N_b and P_b are the electron hole concentrations in the SCH region and N_w and P_w are the electron and hole concentrations in the QW region. J_N and J_P denote the electron and hole injection rates to the SCH layer. The other parameters are given in Table III.

C. Carrier Temperature Dynamic Model

Many interesting and complicated processes occur in QW lasers under high-speed direct current modulation. These include spectral hole burning, interband scattering, carrier-carrier scattering, carrier heating, and carrier recombination due to traps, defects, and other processes [31], [32]. These processes are more or less affected by the carrier capture and carrier transport in the QW heterostructure and lead to the appearance of nonlinearities in gain and related quantities. Therefore, it becomes very important to study these, as they could have a profound effect on wave-guiding and oscillation characteristics of resonantly enhanced QW lasers.

At high modulation frequencies, the carrier distribution in $\boldsymbol{k}$ space changes due to the intraband fluctuations [31]. Restoring forces nullify these distribution variations by carrier–carrier and carrier–phonon scattering [32] and lead to spectral hole burning and carrier heating in QW structures. The finite intraband scattering time and associated rate of establishing quasi-equilibrium in the Fermi distributions leads to spectral hole burning. The carrier heating is due to the combination of injection heating, recombination heating, free carrier absorption heating, and carrier relaxation associated with phonon emissions [32]. We use a density matrix approach [31], [37] to derive carrier temperature equations including the above effects.

By modeling the laser medium as an ensemble of a homogeneously broadened two-level system, we write the following set of density matrix equations for electron ($\rho_{c,k}$) and hole ($\rho_{v,k}$) occupation probabilities in conduction and valence bands and diagonal density matrix element $\rho_{cv,k}$ for the state $\boldsymbol{k}$ [31]:

$$\frac{\partial\rho_{c,k}(t)}{\partial t} = -\frac{\rho_{c,k}(t) - f^c(k,t,T_e)}{\tau_c} - \frac{\rho_{c,k}(t) - f^c(k,t,T_L)}{\tau_{hc}} - \frac{\rho_{c,k}(t) - f^c(k)}{\tau_s} - \frac{i}{\hbar}[\mu_k^*\rho_{cv,k}(t) - \mu_k\rho_{vc,k}(t)]E(z,t) + \Lambda_{c,k} \tag{18}$$

$$\frac{\partial \rho_{v,k}(t)}{\partial t} = -\frac{\rho_{v,k}(t) - f^v(k,t,T_e)}{\tau_v} - \frac{\rho_{v,k}(t) - f^v(k,t,T_L)}{\tau_{hv}} - \frac{\rho_{v,k}(t) - f^v(k)}{\tau_s} - \frac{i}{\hbar}[\mu_k^* \rho_{cv,k}(t) - \mu_k \rho_{vc,k}(t)]E(z,t) + \Lambda_{v,k} \tag{19}$$

$$\frac{\partial \rho_{cv,k}(t)}{\partial t} = \left(-j\omega_k - \frac{1}{\tau}\right)\rho_{cv,k}(t) - \frac{j}{\hbar}\mu_k[\rho_{c,k}(t) + \rho_{v,k}(t) - 1]E(z,t) \tag{20}$$

$$\rho_{vc,k} = \rho_{cv,k}^* \tag{21}$$

where $\{f^\alpha(k,t,T_\beta)\colon \alpha \in \{c,v\}, \beta \in \{e,h,L\}\}$ are the instantaneous Fermi functions for the conduction and valence bands at designated carrier temperatures $\{T_\beta\colon \beta \in \{e,h,L\}\}$, $f^c(k)$ and $f^v(k)$ are the Fermi distributions at thermal equilibrium for the conduction and valence bands, τ_{ch} and τ_{vh} are the carrier–phonon interaction times for conduction and valence bands, $\Lambda_{c,k}$ and $\Lambda_{v,k}$ are the injection rates into the conduction and valence bands, and μ_k is the dipole moment of the transitions between the conduction and valence bands at $\boldsymbol{k}$ state. Suppose U_c and U_v are the energy densities for electrons and holes in conduction and valence bands. Then, using (16)–(21), we can derive the following equations for evolution of energy densities $U_c(T)$ and $U_v(T)$ at temperatures $T = T_e$ and $T = T_h$, respectively, for electrons and holes:

$$\frac{dU_c}{dt} = \Delta E_{\text{inj}}^c J_{Nw} - \Delta E_{\text{stim}}^c V_g G I + \hbar\omega_s V_g \alpha_{fca}^c I N_w - \frac{U_c(T_e) - U_c(T_L)}{\tau_{hc}} - \Delta E_{\text{rec}}^c \left(\frac{N_w P_w}{\tau_{\text{spn}} P_w + \tau_{\text{spp}} N_w} + B N_w P_w + C_N N_w^2 P_w + C_P N_w P_w^2\right) \tag{22}$$

$$\frac{dU_v}{dt} = \Delta E_{\text{inj}}^v J_{Pw} - \Delta E_{\text{stim}}^v V_g G I + \hbar\omega_s V_g \alpha_{fca}^v I P_w - \frac{U_v(T_h) - U_v(T_L)}{\tau_{hv}} - \Delta E_{\text{rec}}^v \left(\frac{N_w P_w}{\tau_{\text{spn}} P_w + \tau_{\text{spp}} N_w} + B N_w P_w + C_N N_w^2 P_w + C_P N_w P_w^2\right) \tag{23}$$

where ΔE_{inj}^c and ΔE_{inj}^v are the average injection heating energies for electrons and holes, ΔE_{stim}^c and ΔE_{stim}^v are the average stimulated recombination heating energies for electrons and holes and ΔE_{rec}^c and ΔE_{rec}^v are the average energies associated with nonstimulated recombination heating for electrons and holes. J_{Nw} and J_{Pw} denote the net injection rates into the active medium. The other parameters are given in Table I. Considering the dependence of $U_c(T)$ and $U_v(T)$ on corresponding carrier temperatures and carrier distributions in conduction and valence bands, we can write the following functional relationships:

$$\frac{dU_c}{dt} = \frac{\partial U_c}{\partial T_e}\frac{dT_e}{dt} + \frac{\partial U_c}{\partial N_w}\frac{dN_w}{dt} \tag{24}$$

$$\frac{dU_v}{dt} = \frac{\partial U_v}{\partial T_h}\frac{dT_h}{dt} + \frac{\partial U_v}{\partial P_w}\frac{dP_w}{dt} \tag{25}$$

and substituting expressions for $\frac{dU_c}{dt}$, $\frac{dU_v}{dt}$, $\frac{dN_w}{dt}$, and $\frac{dP_w}{dt}$ from (16), (17), (22), and (23), we can derive the following equations for the carrier temperature fluctuations in electrons and holes:

$$\frac{dT_e}{dt} = \left(\frac{\partial U_c}{\partial T_e}\right)^{-1} \cdot \left[\left(\Delta E_{\text{inj}}^c - \frac{\partial U_c}{\partial N_w}\right)\left(\frac{V_b}{V_w}\frac{N_b}{\tau_{bwn}} - \frac{N_w}{\tau_{wbn}}\right) + \left(\frac{\partial U_c}{\partial N_w} - \Delta E_{\text{stim}}^c\right)V_g G I + \left(\frac{\partial U_c}{\partial N_w} - \Delta E_{\text{rec}}^c\right) \cdot \left(\frac{N_w P_w}{\tau_{spn} P_w + \tau_{spp} N_w} + B N_w P_w + C_N N_w^2 P_w + C_P N_w P_w^2\right) + \hbar\omega_s V_g \alpha_{fca}^c I N_w - \frac{U_c(T_e) - U_c(T_L)}{\tau_{hc}}\right] \tag{26}$$

$$\frac{dT_h}{dt} = \left(\frac{\partial U_v}{\partial T_h}\right)^{-1} \cdot \left[\left(\Delta E_{\text{inj}}^v - \frac{\partial U_v}{\partial P_w}\right)\left(\frac{V_b}{V_w}\frac{P_b}{\tau_{bwp}} - \frac{P_w}{\tau_{wbp}}\right) + \left(\frac{\partial U_v}{\partial P_w} - \Delta E_{\text{stim}}^v\right)V_g G I + \left(\frac{\partial U_v}{\partial P_w} - \Delta E_{\text{rec}}^v\right) \cdot \left(\frac{N_w P_w}{\tau_{spn} P_w + \tau_{spp} N_w} + B N_w P_w + C_N N_w^2 P_w + C_P N_w P_w^2\right) + \hbar\omega_s V_g \alpha_{fca}^v I P_w - \frac{U_v(T_h) - U_v(T_L)}{\tau_{hv}}\right]. \tag{27}$$

This completes the derivation of the system of equations governing the time evolution of the QW laser with Bragg grating external cavity. We use above equations in next section to find the small-signal modulation performance of this system.

D. Small-Signal Modulation Response

To calculate the small-signal modulation response, we carry out a perturbation analysis around a steady-state oscillation mode. Steady-state solutions can be found by solving (2), (3), (14)–(17), (26), and (27) self-consistently, considering the gain and the round-trip phase conditions. The Appendix gives the resulting transfer matrix after Fourier transforming the perturbation expanded system.

The interrelationship between different small-signal quantities are visually depicted in Fig. 6(a). It shows that the external cavity induces both self- and cross-coupling between intensity fluctuations ΔI and phase fluctuations, $\Delta\varphi$. The intensity and phase fluctuations are also coupled indirectly through QW electron and hole density fluctuations ΔN_w and ΔP_w and SCH electron and hole fluctuations, ΔN_b and ΔP_b, respectively. The direct links between ΔN_w, ΔP_w, and $\Delta\varphi$ show the direct influence of the QW carrier fluctuations on the optical field phase through the linewidth enhancement factor. The direct

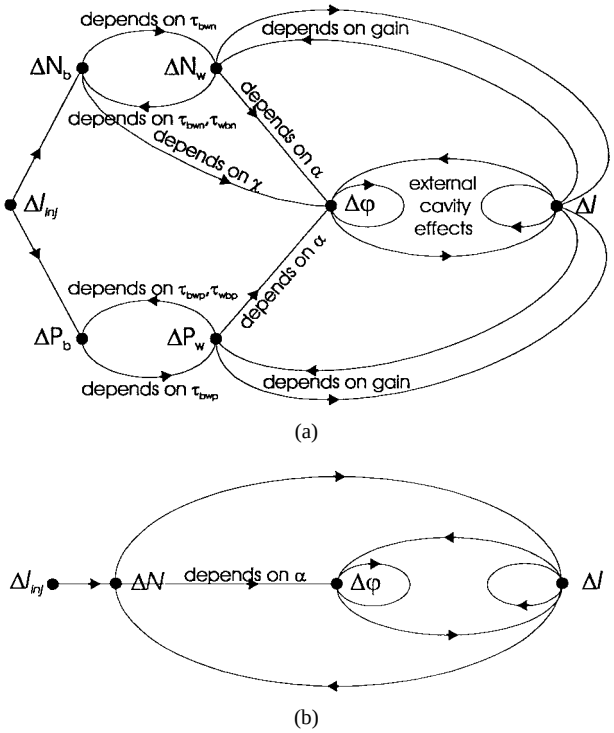

Fig. 6. Signal flow graphs for strong feedback external cavity laser with (a) QW active layer and (b) bulk active layer.

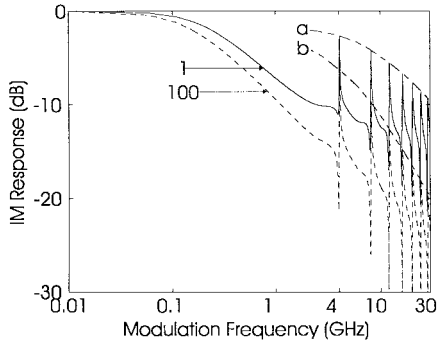

Fig. 7. Intensity modulation response for the fiber grating external cavity laser with 4-GHz external-cavity resonance frequency for two carrier transport times 1 and 100 ps. Cavity-resonance-peak loci for 1- and 100-ps carrier transport times are drawn as **a** and **b**, respectively. Note the resonance enhanced response close to multiples of the external-cavity resonance frequency and nulls appearing close to them.

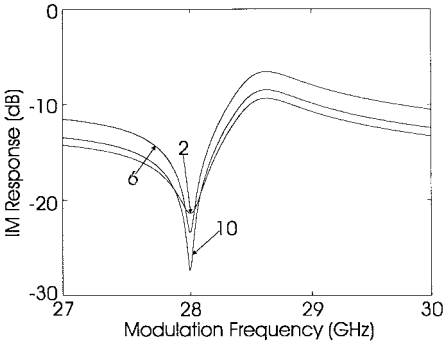

Fig. 8. IM response against the modulation frequency as the SCH phase coupling constant for three χ (10^{-14} rad·m^{-3}·s^{-1}) values. It shows the increase of null depth as χ increases.

link between SCH electron density fluctuations, ΔN_b and $\Delta\varphi$, shows that the phase of the lasing field is also directly affected by the SCH carrier fluctuations due to its significant contribution to the waveguiding. However, the electron–electron and hole–hole distributions in the SCH and QW are also coupled through feedback paths. Therefore, electron and hole density fluctuations in the SCH region have an indirect influence on the phase of the optical field. As the intensity fluctuation ΔI is coupled directly with electron and hole fluctuations using feedforward and feedback paths, the fluctuations in the SCH and QW are reflected in ΔI fluctuations. However, due to the different coupling paths, they experience different delays and, hence, different characteristic times. The nonlinear interaction of these carrier-phase-intensity fluctuations leads to the modification of the high-speed modulation response as shown in Section III (see Figs. 7–12). Fig. 6(b) shows the signal flow diagram for the bulk laser with strong external feedback for comparison [9].

III. Resonantly Enhanced Response

We use the data given in Table I for our simulations. The photon and carrier density rate equations were solved self-consistently until a solution is reached to find a steady-state operating point. In [9], we showed that the resonant enhancement in bulk active layer lasers depends on the bias level, linewidth enhancement factor, intermediate facet reflectivity, external feedback level, external cavity length, and nonlinear gain coefficient associated with spectral hole burning. It can be shown using the theory presented here that the above qualitative relationships still hold for strong feedback external cavity lasers with QW active layers. Therefore, we omit this information in this paper and refer the reader to [9] for details.

Here, we concentrate our analysis on the seventh harmonic resonance frequency (i.e., ∼30 GHz) of a 4-GHz external-cavity laser with a Bragg reflector. Fig. 7 shows the inensity modulation (IM) response of this laser electron-carrier-transport times of 1 and 100 ps. It shows that the resonance peaks appear at 4-GHz intervals, and their amplitudes decrease at high frequencies due to carrier transport effects. This can be clearly seen by comparing the resonance peak loci **a** and **b** for the 1- and 100-ps carrier transport times, respectively. The nulls close to the resonance peaks result from the amplitude-phase coupling caused by the interplay between the laser cavity and the external cavity [9]. Careful inspection of (3) shows that in the QW the amplitude-phase coupling results from two parameters:

i) the linewidth enhancement factor α_{gsp};
ii) the parameter χ representing refractive index modulation in the SCH region.

Fig. 8 shows the IM response close to seventh harmonic resonance peak as χ varies. It shows that larger χ leads to deeper nulls close to the external-cavity resonance frequency. To understand this, we consider (1) and write following expression for single-pass phase change rate through active

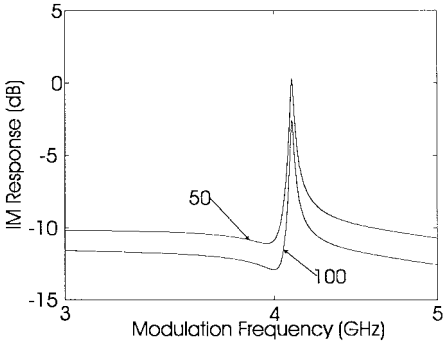

Fig. 9. IM response against the modulation frequency for two hole transport times τ_{bwp} (ps). This shows the response around fundamental resonance frequency for a 4 GHz cavity. Observe that only the damping rate is affected significantly. The null depth has minimal sensitivity to τ_{bwp}.

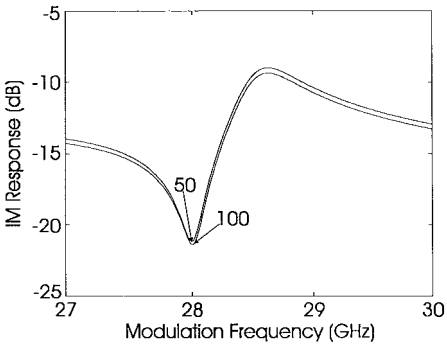

Fig. 10. IM response against the modulation frequency as for two hole transport times τ_{bwp} (ps). This shows the response around seventh harmonic resonance frequency for a 4 GHz cavity. Observe that damping rate and null depth have insignificant sensitivity to τ_{bwp}.

region (excluding external cavity effects) as [47], [57]:

$$\left.\frac{d\varphi}{dt}\right|_{\substack{\text{single pass}\\ \text{in QW layer}}} = \frac{2\pi c}{\lambda n_{\text{eff}}}\left[\Gamma\frac{dn_{\text{eff}w}}{dN_w}\Delta N_w + (1-\Gamma)\frac{dn_{\text{eff}b}}{dN_b}\Delta N_b\right]$$
$$= \tfrac{1}{2}\Gamma\alpha_{gsp}\Delta G + (1-\Gamma)\chi x\Delta N_b \qquad (28)$$

where ΔG is the gain perturbation and $\chi = (2\pi c/\lambda n_{\text{eff}})(dn_{\text{eff}b}/dN_b)$. The other parameter definitions are given in Table I. This observation suggests that χ behaves similarly to the linewidth enhancement factor in bulk lasers. Therefore, the advantage of using QW lasers for a reduced linewidth enhancement factor is nullified by this factor. It can also be shown that carrier transport effects lead to the modification of this phase change and hence the amount of chirping [47]. Considering solitary QW lasers, Nagarajan *et al.* [47] showed that the SCH differential refractive index's $(\partial n_{\text{eff}b}/\partial N_b)$ influence on chirping is modified by a factor of carrier transport to carrier escape times in the QW and the maximum injection into the active region. However, their result is expected to be modified here due to strong frequency-selective feedback due to the external cavity. Detailed studies by Yamada *et al.* [58] showed that amplitude-phase coupling can be decreased by using potential-controlled or modulation-doped MQW structures [59], [60]. In these structures, the barriers were heavily doped with p-type impurities. This technique could be used in our lasers.

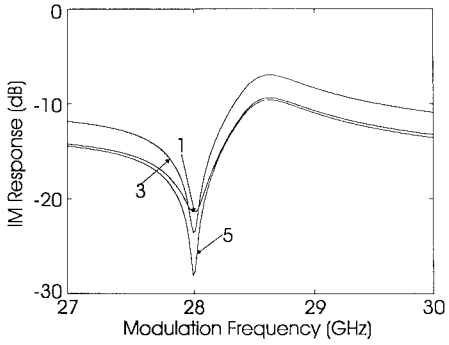

Fig. 11. IM response against the modulation frequency for three electron transport times τ_{bwn} (picoseconds). This shows that the null depth is highly sensitive to the electron transport time.

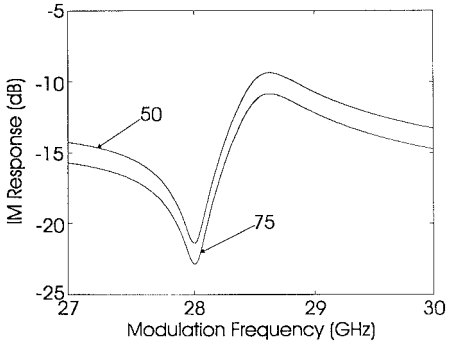

Fig. 12. IM response against the modulation frequency for two electron escape times τ_{wbn} (picoseconds). This shows that electron escape time influences the modulation response level but has no significant effect on the null characteristics.

Figs. 9 and 10 show the variation of IM response against the modulation frequency close to the fundamental and seventh harmonic resonance peak for two carrier transport times of holes (τ_{bwp}). Comparison shows that the hole transport time only reduces the modulation efficiency. Further, this effect is very weak and diminishes as the harmonic number increases. In contrast, the electron transport time has a very significant effect on the modulation response. Fig. 11 shows the IM response around the seventh harmonic, when the electron transport time τ_{bwn} is varied. It shows that depth of the null close to harmonic of the external-cavity resonance frequency is highly sensitive to the electron transport time τ_{bwn}. The difference in effect of the electron and hole transport times can be explained by the high effective mass of holes relative to electrons; the holes' contribution to the amplitude phase coupling is diminished under high-speed modulation as they react slowly to dynamic fluctuations due to their inertia. The carrier transport times can be reduced by properly designing the SCH regions [56]. Fig. 12 shows that the electron escape time τ_{wbn} from the QW has no significant influence on the null depth. However, it shows the modulation response level is slightly decreased for increasing τ_{wbn}. A similar analysis on hole escape time from the QW shows that it has no significant effect on null depth or modulation response level.

IV. Discussion

To understand the influence of carrier transport related small-signal response modification, we can analyze the re-

$$\Pi_{11} = \Gamma I_s \frac{\partial G}{\partial I} + \Gamma G_s - \alpha_L + \ln(R_1 R_2)/\tau_L + 2\frac{H_1}{\tau_L} - \frac{P_2}{\tau_L}[1 - \exp(-j\Omega\tau)] + j\Omega$$

$$\Pi_{12} = -2\frac{I_s}{\tau_L}[1 - \exp(-j\Omega\tau)]H_2; \qquad \Pi_{13} = 0; \qquad \Pi_{14} = 0; \qquad \Pi_{15} = \Gamma I_s \frac{\partial G}{\partial N_w} + \Gamma\beta B P_{ws};$$

$$\Pi_{16} = \Gamma I_s \frac{\partial G}{\partial P_w} + \Gamma\beta B N_{ws}; \qquad \Pi_{17} = \Gamma I_s \frac{\partial G}{\partial T_e}\Delta T_e; \qquad \Pi_{18} = \Gamma I_s \frac{\partial G}{\partial T_h}\Delta T_h$$

$$\Pi_{21} = 0.5\Gamma\alpha_{gsp}\frac{\partial G}{\partial I} + \left(\frac{H_2 - 2P_2}{2I_s\tau_L}\right)[1 - \exp(-j\Omega\tau)];$$

$$\Pi_{22} = \left(\frac{\alpha_{gsp}\Gamma H_2 + P_2}{\tau_L}\right)[1 - \exp(-j\Omega\tau)] + j\Omega; \qquad \Pi_{23} = (1-\Gamma)\chi; \qquad \Pi_{24} = 0;$$

$$\Pi_{25} = 0.5\Gamma\alpha_{gsp}\frac{\partial G}{\partial N_w}; \qquad \Pi_{26} = 0.5\Gamma\alpha_{gsp}\frac{\partial G}{\partial P_w}; \qquad \Pi_{27} = 0.5\Gamma\alpha_{gsp}\frac{\partial G}{\partial T_e}\Delta T_e$$

$$\Pi_{28} = 0.5\Gamma\alpha_{gsp}\frac{\partial G}{\partial T_h}\Delta T_h; \quad \Pi_{31} = -\left(G_s + I_s\frac{\partial G}{\partial I}\right); \quad \Pi_{32} = 0; \quad \Pi_{33} = \frac{V_b}{V_w}\frac{1}{\tau_{bwn}}; \quad \Pi_{34} = 0$$

$$\Pi_{35} = -\left[\frac{1}{\tau_{wbn}} + I_s\frac{\partial G}{\partial N_w} + \frac{\tau_{spn}P_{ws}^2}{(\tau_{spn}P_{ws}^2 + \tau_{spp}N_{ws}^2)^2} + BP_{ws} + 2C_nN_{ws}P_{ws} + C_pP_{ws}^2\right] + j\Omega$$

$$\Pi_{36} = -\left[I_s\frac{\partial G}{\partial P_w} + \frac{\tau_{spp}N_{ws}^2}{(\tau_{spn}P_{ws}^2 + \tau_{spp}N_{ws}^2)^2} + BN_{ws} + C_nN_{ws}^2 + 2C_pN_{ws}P_{ws}\right]; \qquad \Pi_{37} = -I_s\frac{\partial G}{\partial T_e};$$

$$\Pi_{38} = -I_s\frac{\partial G}{\partial T_h}; \qquad \Pi_{41} = -\left(G_s + I_s\frac{\partial G}{\partial I}\right); \qquad \Pi_{42} = 0; \qquad \Pi_{43} = 0; \qquad \Pi_{44} = \frac{V_b}{V_w}\frac{1}{\tau_{bwp}};$$

$$\Pi_{45} = -\left[I_s\frac{\partial G}{\partial N_w} + \frac{\tau_{spn}P_{ws}^2}{(\tau_{spn}P_{ws}^2 + \tau_{spp}N_{ws}^2)^2} + BP_{ws} + 2C_nN_{ws}P_{ws} + C_pP_{ws}^2\right]$$

$$\Pi_{46} = -\left[\frac{1}{\tau_{wbp}} + I_s\frac{\partial G}{\partial P_w} + \frac{\tau_{spp}N_{ws}^2}{(\tau_{spn}P_{ws}^2 + \tau_{spp}N_{ws}^2)^2} + BN_{ws} + C_nN_{ws}^2 + 2C_pN_{ws}P_{ws}\right] + j\Omega$$

$$\Pi_{47} = -I_s\frac{\partial G}{\partial T_e}; \qquad \Pi_{48} = -I_s\frac{\partial G}{\partial T_h}; \qquad \Pi_{51} = 0; \qquad \Pi_{52} = 0; \qquad \Pi_{53} = -\frac{1}{\tau_{bwn}};$$

$$\Pi_{54} = 0; \qquad \Pi_{55} = \frac{V_w}{V_b}\frac{1}{\tau_{wbn}}; \qquad \Pi_{56} = 0; \qquad \Pi_{57} = 0; \qquad \Pi_{58} = 0; \qquad \Pi_{61} = 0;$$

$$\Pi_{62} = 0; \qquad \Pi_{63} = 0; \qquad \Pi_{64} = -\frac{1}{\tau_{bwp}}; \qquad \Pi_{65} = 0; \qquad \Pi_{66} = \frac{V_w}{V_b}\frac{1}{\tau_{wbp}}; \qquad \Pi_{67} = 0;$$

$$\Pi_{68} = 0; \qquad \Pi_{71} = \left(\frac{\partial U_c}{\partial T_e}\right)^{-1}\left[\left(\frac{\partial U_c}{\partial N_w} - \Delta E_{\text{stim}}^c\right)\left(G_s + I_s\frac{\partial G}{\partial I}\right) + \hbar\omega_s V_g\alpha_{fca}^c N_{ws}\right];$$

$$\Pi_{72} = 0; \qquad \Pi_{73} = \left(\frac{\partial U_c}{\partial T_e}\right)^{-1}\left[\left(\Delta E_{\text{inj}}^c - \frac{\partial U_c}{\partial N_w}\right)\frac{V_b}{V_w}\frac{1}{\tau_{bwn}}\right]; \qquad \Pi_{74} = 0$$

$$\Pi_{75} = \left(\frac{\partial U_c}{\partial T_e}\right)^{-1}\left\{-\left(\Delta E_{\text{inj}}^c - \frac{\partial U_c}{\partial N_w}\right)\frac{1}{\tau_{wbn}} + \left(\frac{\partial U_c}{\partial N_w} - \Delta E_{\text{stim}}^c\right)I_s\frac{\partial G}{\partial N_w} + \hbar\omega_s V_g\alpha_{fca}^c I_s - \frac{\partial U_c}{\partial N_w}\frac{1}{\tau_{hc}}\right.$$
$$\left.\cdot\left(\frac{\partial U_c}{\partial N_w} - \Delta E_{\text{rec}}^c\right)\left[\frac{\tau_{spn}P_{ws}^2}{(\tau_{spn}P_{ws} + \tau_{spp}N_{ws})^2} + BP_{ws} + 2C_nN_{ws}P_{ws} + C_pP_{ws}^2\right]\right\}$$

$$\Pi_{76} = \left(\frac{\partial U_c}{\partial T_e}\right)^{-1}\left\{\left(\frac{\partial U_c}{\partial N_w} - \Delta E_{\text{stim}}^c\right)I_s\frac{\partial G}{\partial P_w} + \left(\frac{\partial U_c}{\partial N_w} - \Delta E_{\text{rec}}^c\right)\right.$$
$$\left.\cdot\left[\frac{\tau_{spp}N_{ws}^2}{(\tau_{spn}P_{ws} + \tau_{spp}N_{ws})^2} + BN_{ws} + C_nN_{ws}^2 + 2C_pN_{ws}P_{ws}\right]\right\}$$

$$\Pi_{77} = \left(\frac{\partial U_c}{\partial T_e}\right)^{-1}\left[\left(\frac{\partial U_c}{\partial N_w} - \Delta E_{\text{stim}}^c\right)I_s\frac{\partial G}{\partial T_e} - \frac{\partial U_c}{\partial T_e}\frac{1}{\tau_{hc}}\right] + j\Omega;$$

$$\Pi_{78} = \left(\frac{\partial U_c}{\partial T_e}\right)^{-1}\left[\left(\frac{\partial U_c}{\partial N_w} - \Delta E_{\text{stim}}^c\right)I_s\frac{\partial G}{\partial T_h}\right]$$

$$\Pi_{81} = \left(\frac{\partial U_v}{\partial T_h}\right)^{-1}\left[\left(\frac{\partial U_v}{\partial P_w} - \Delta E_{\text{stim}}^v\right)\left(G_s + I_s\frac{\partial G}{\partial I}\right) + \hbar\omega_s V_g\alpha_{fca}^v P_{ws}\right]$$

$$\Pi_{82}=0;\qquad \Pi_{83}=0;\qquad \Pi_{84}=\left(\frac{\partial U_v}{\partial T_h}\right)^{-1}\left[\left(\Delta E^v_{\rm inj}-\frac{\partial U_v}{\partial P_w}\right)\frac{V_b}{V_w}\,\frac{1}{\tau_{bwp}}\right];$$

$$\Pi_{85}=\left(\frac{\partial U_v}{\partial T_h}\right)^{-1}\left\{\left(\frac{\partial U_c}{\partial P_w}-\Delta E^v_{\rm stim}\right)I_s\frac{\partial G}{\partial N_w}+\left(\frac{\partial U_v}{\partial P_w}-\Delta E^v_{\rm rec}\right)\cdot\left[\frac{\tau_{spn}P^2_{ws}}{(\tau_{spn}P_{ws}+\tau_{spp}N_{ws})^2}+BP_{ws}+2C_nN_{ws}P_{ws}+C_pP^2_{ws}\right]\right\}$$

$$\Pi_{86}=\left(\frac{\partial U_v}{\partial T_h}\right)^{-1}\left\{-\left(\Delta E^v_{\rm inj}-\frac{\partial U_v}{\partial P_w}\right)\frac{1}{\tau_{wbp}}+\left(\frac{\partial U_v}{\partial P_w}-\Delta E^v_{\rm stim}\right)I_s\frac{\partial G}{\partial P_w}+\hbar\omega_sV_g\alpha^v_{fca}I_s-\frac{\partial U_v}{\partial P_w}\,\frac{1}{\tau_{hv}}\cdot\left(\frac{\partial U_v}{\partial P_w}-\Delta E^v_{\rm rec}\right)\left[\frac{\tau_{spp}N^2_{ws}}{(\tau_{spn}P_{ws}+\tau_{spp}N_{ws})^2}+BN_{ws}+C_nN^2_{ws}+2C_pN_{ws}P_{ws}\right]\right\}$$

$$\Pi_{87}=\left(\frac{\partial U_v}{\partial T_h}\right)^{-1}\left[\left(\frac{\partial U_v}{\partial P_w}-\Delta E^v_{\rm stim}\right)I_s\frac{\partial G}{\partial T_e}\right];$$

$$\Pi_{88}=\left(\frac{\partial U_v}{\partial T_h}\right)^{-1}\left[\left(\frac{\partial U_v}{\partial P_w}-\Delta E^v_{\rm stim}\right)I_s\frac{\partial G}{\partial T_h}-\frac{\partial U_v}{\partial T_h}\,\frac{1}{\tau_{hv}}\right]+j\Omega$$

action of the composite system for a small perturbation in carrier density in the SCH or QW regions. Without loss of generality, we consider a small fluctuation in SCH electron density ΔN_b. The signal flow graph in Fig. 6(a) shows that this carrier fluctuation leads to the activation of eighteen feedback loops. The equilibrium state of the fluctuations in these feedback loops represent the appearance of resonance peaks, nulls, modulation efficiency changes, and the broadening of resonance peaks.

It is interesting to compare these carrier fluctuation initiated feedback effects with the corresponding response of a bulk laser. Using Fig. 6(b), we deduce that in a bulk laser, only three feedback loops are initiated due to any carrier fluctuation, namely $\{\Delta N\rightarrow\Delta I\rightarrow\ \Delta N\}$, $\{\Delta N\rightarrow\Delta I\rightarrow\Delta\varphi\rightarrow\Delta I\rightarrow\Delta N\}$, and $\{\Delta N\rightarrow\ \Delta\varphi\ \rightarrow\ \Delta I\rightarrow\ \Delta N\}$. Careful inspection of these three loops shows that strong amplitude-phase coupling [$\Delta I\Leftrightarrow\Delta\varphi$: the middle loop in Fig. 6(a) and (b)] is vital to maintain any significant contribution to the small-signal response. We showed in [9] that the linewidth enhancement factor and the intermediate facet reflectivity have a direct influence on the loop gains of these feedback loops. However, inspection of the feedback loops associated with the QW active layer shows that, in the absence of bidirectional amplitude-phase coupling results from linewidth enhancement factor and external cavity [see Fig. 6(a)], there exist twelve feedback loops with significant gain due to carrier transport. Therefore, spectral anomalies (i.e., nulls and resonance peaks: see Figs. 7–12) are still possible depending on the interaction levels of the different feedback loops and associated relaxation times. Another important observation of the feedback loops of the quantum well laser is that any amplitude-phase coupling due the to SCH layer has to be through two main signal flow branches $\Delta N_b\leftrightarrow\Delta N_w$ and $\Delta N_b\rightarrow\Delta\varphi$. The gains of these two branches are mostly controlled by the electron carrier transport time τ_{bwn} and the SCH layer related linewidth enhancement-type factor χ. In our simulations, we saw that the small-signal response is mostly sensitive to these two factors than to any other parameters used in the model.

V. Conclusion

A detailed model for fiber grating external-cavity lasers with QW active regions has been developed. Carrier transport, carrier heating, intraband carrier fluctuations, and nonparabolic band structure effects were considered. We showed that incorporation of a QW active layer leads to unique dependencies of resonant enhancement effects not seen in bulk lasers. In a previous study [9], we showed that the reduction of linewidth enhancement factor in bulk lasers leads to the suppression of nulls close to the resonance peaks. As QW lasers have reduced linewidth enhancement factors, we could have expected them to have wide-bandwidth resonance peaks due to the suppression of the nulls close to them. However, in this paper, we have shown that a reduction of linewidth enhancement factor is not enough to achieve this, because amplitude-phase coupling also occurs due to carrier fluctuations in the SCH region modulating its refractive index. We also showed that the small-signal response is affected more significantly by carrier transport times than carrier capture times.

Appendix

To calculate the noise and small-signal response, we take the Fourier transform of the perturbation expanded equations and obtain the following form:

$$\Pi(\Omega)\Xi(\Omega)=\Theta_M \tag{A1}$$

for modulation response and

$$\Pi(\Omega)\Xi(\Omega)=\Theta_N \tag{A2}$$

for the noise response. If the variation of intensity, phase, SCH carrier densities, QW carrier densities, and carrier tempera-

tures from the steady state are $\Delta I e^{j\Omega t}$, $\Delta\varphi e^{j\Omega t}$, $\Delta N_b e^{j\Omega t}$, $\Delta P_b e^{j\Omega t}$, $\Delta N_w e^{j\Omega t}$, $\Delta P_w e^{j\Omega t}$, $\Delta T_e e^{j\Omega t}$, and $\Delta T_h e^{j\Omega t}$ at modulation angular frequency Ω, then we can write the following expressions for the coefficients for $\Xi(\Omega)$, $\Pi(\Omega)$ as follows:

$$\Xi(\Omega) = [\Delta I, \Delta\varphi, \Delta N_w, \Delta P_w, \Delta N_b, \Delta P_b, \Delta T_e, \Delta T_h]^T \tag{A3}$$

and if $\Pi(\Omega) = \{\Pi_{mn}\colon m, n \in [1, 8], m, n\{$ integers$\}$ and assuming gain G can be written to first order as $G = G_s + \frac{\partial G}{\partial I}\Delta I e^{j\Omega t} + \frac{\partial G}{\partial N_w}\Delta N_w e^{j\Omega t} + \frac{\partial G}{\partial P_w}\Delta P_w e^{j\Omega t} + \frac{\partial G}{\partial T_e}\Delta T_e e^{j\Omega t} + \frac{\partial G}{\partial T_h}\Delta T_h e^{j\Omega t}$ where derivatives are understood to be evaluated at steady-state values (to simplify the notation). Then, the coefficients can be written as shown on the two previous pages.

If the modulation current fluctuation from steady state is given as $\Delta I_{\mathrm{inj}} e^{j\Omega t}$ then we can write Θ_M as

$$\Theta_M = (\Delta I_{\mathrm{inj}}/qV_{sch})[0, 0, 1, 1, 0, 0, 0, 0]^T. \tag{A4}$$

Similarly, considering Langevian noise sources for amplitude and phase, we can write the following expression for Θ_N:

$$\Theta_N = [F_I, F_\varphi, 0, 0, 0, 0, 0, 0] \tag{A5}$$

where $\langle F_I F_I^* \rangle = R(2I_s + 1)$, $\langle F_\varphi F_\varphi^* \rangle = R/2I_s$, and $\langle F_I F_\varphi^* \rangle = \langle F_I^* F_\varphi \rangle = 0$. R denotes the spontaneous emission rate into the cavity. Solving these matrices for required arguments, we can calculate the noise and modulation response for this system.

ACKNOWLEDGMENT

The authors appreciate the help given by Assoc. Prof. Y. Hua, A. Nirmalathas, J. Yates, and Dr. J. Badcock.

REFERENCES

[1] A. S. Daryoush, "Optical synchronization of millimeter-wave oscillators for distributed architectures," *IEEE Trans. Microwave Theory Tech.*, vol. 38, pp. 467–476, May 1990.

[2] P. J. Heim and C. P. McClay, "Frequency division multiplexed microwave and baseband digital optical fiber link for phased array antennas," *IEEE Trans. Microwave Theory Tech.*, vol. 38, pp. 494–500, May 1990.

[3] S. Levy, R. Nagarajan, A. Mar, P. Humphrey, and J. E. Bowers, "Fiber-optic PSK subcarrier transmission at 35 GHz using a resonantly enhanced semiconductor laser," *Electron. Lett.*, vol. 28, pp. 2103–2104, Oct. 1992.

[4] S. Levy, R. Nagarajan, R. J. Helkey, P. Humphrey, and J. E. Bowers, "Millimeter wave fiber-optic PSK subcarrier transmission at 35 GHz over 6.3 km using a grating external cavity semiconductor laser," *Electron. Lett.*, vol. 29, pp. 690–691, Apr. 1993.

[5] R. Nagarajan, S. Levy, A. Mar, and J. E. Bowers, "Resonantly enhanced semiconductor laser for efficient transmission of millimeter wave modulated light," *IEEE Photon. Technol. Lett.*, vol. 5, pp. 4–6, Jan. 1993.

[6] L. Zhang and D. A. Ackerman, "Second- and third-order harmonic distortion in DFB lasers," *IEEE J. Quantum Electron.*, vol. 31, pp. 1974–1980, Nov. 1995.

[7] R. Nagarajan, S. Levy, and J. E. Bowers, "Millimeter wave narrowband optical fiber links using external cavity semiconductor lasers," *J. Lightwave Technol.*, vol. 12, pp. 127–136, Jan. 1994.

[8] J. B. Georges, M. H. Kiang, K. Heppell, M. Sayed, and K. Y. Lau, "Optical transmission of narrow-band millimeter-wave signals by resonant modulation of monolithic semiconductor laser," *IEEE Photon. Technol. Lett.*, vol. 6, pp. 568–570, Apr. 1994.

[9] M. Premaratne, A. J. Lowery, Z. Ahmed, and D. Novak, "Modeling noise and modulation performance of fiber grating external cavity lasers," *IEEE J. Select. Topics Quantum Electron.*, vol. 3, pp. 290–303, 1997.

[10] C. T. Sullivan, W. S. C. Chang, and R. X. Lu, in *Proc. 10th Anniversary Nat. Science Foundation Grantee-User Meet. on Optical Communication Systems*, J. R. Whiney, Ed. Berkeley, CA: University of California Berkeley, 1982, pp. 28–32.

[11] J. M. Hammer, C. C. Neil, N. W. Carlson, M. T. Duffy, and J. M. Shaw, "Single-wavelength operation of the hybrid-external Bragg reflector waveguide laser under dynamic conditions," *Appl. Phys. Lett.*, vol. 47, pp. 183–185, Aug. 1985.

[12] P. A. Morton, V. Mizrahi, P. A. Andrekson, T. Tanbun-Ek, R. A. Logan, D. L. Coblentz, A. M. Sergent, and K. W. Wecht, "Hybrid soliton pulse source with fiber external cavity and Bragg reflector," *Electron. Lett.*, vol. 28, pp. 561–562, 1992.

[13] Z. Ahmed and R. S. Tucker, "Small-signal IM response of grating-terminated external cavity semiconductor lasers," *IEEE J. Select. Topics Quantum Electron.*, vol. 1, pp. 505–515, June 1995.

[14] G. P. Agrawal and N. K. Dutta, *Long-Wavelength Semiconductor Lasers.* New York: Van Nostrand Reinhold, 1986.

[15] N. A. Olsson, C. H. Henry, R. F. Kazarinov, H. J. Lee, and K. J. Orlowsky, "Performance characteristics of a 1.5 μm single frequency semiconductor laser with an external waveguide Bragg reflector," *IEEE J. Quantum Electron.*, vol. 24, pp. 143–147, Feb. 1988.

[16] N. Holonyak, Jr., R. M. Kolbas, R. D. Dupuis, and P. D. Dapkus, "Quantum well heterostructure lasers," *IEEE J. Quantum Electron.*, vol. QE-16, pp. 170–185, Feb. 1980.

[17] Y. Arakawa and A. Yariv, "Quantum well lasers-gain, spectra, dynamics," *IEEE J. Quantum Electron.*, vol. QE-22, pp. 1887–1899, Sept. 1986.

[18] H. Okamoto, "Semiconductor quantum well structure for optoelectronics—Recent advances and future prospects," *Jpn. J. Appl. Phys.*, vol. 26, pp. 315–330, Mar. 1987.

[19] R. W. Tkach and A. R. Charplyvy, "Regimes of feedback effects in 1.5 μm distributed feedback laser," *J. Lightwave Technol.*, vol. 8, pp. 512–518, 1986.

[20] P. Besnard, B. Meziane, and G. M. Stephan, "Feedback phenomena in a semiconductor laser induced by distant reflectos," *IEEE J. Quantum Electron.*, vol. 29, pp. 1271–1284, May 1993.

[21] M. F. Ferreira, J. F. Rocha, and J. L. Pinto, "Noise and modulation performance of Fabry–Perot and DFB semiconductor lasers with arbitrary external optical feedback," *Proc. Inst. Elect. Eng.*, vol. 137, pt. J, pp. 361–369, Dec. 1990.

[22] R. Lang and K. Kobayashi, "External optical feedback effects on semiconductor injection laser properties," *IEEE J. Quantum Electron.*, vol. QE-16, pp. 347–355, Mar. 1980.

[23] R. Nagarajan and J. E. Bowers, "Effects of carrier transport on injection efficiency and wavelength chirping in quantum well lasers," *IEEE J. Quantum Electron.*, vol. 29, pp. 1601–1608, June 1993.

[24] N. Tessler and G. Eisentein, "On carrier injection and gain dynamics in quantum well lasers," *IEEE J. Quantum Electron.*, vol. 29, pp. 1586–1595, June 1993.

[25] N. Tessler, R. Nagar, and G. Eisenstein, "Structure dependent modulation response in quantum well lasers," *IEEE J. Quantum Electron.*, vol. 28, pp. 2242–2250, Oct. 1992.

[26] M. Premaratne and A. J. Lowery, "Design of single-mode high-efficiency fiber grating external cavity lasers," in *Proc. 21st Australian Conf. on Optical Fiber Technology (ACOFT-21'96)*, Gold Coast, Queensland, Australia, Dec. 1996, pp. 171–174.

[27] S. H. Park, J. I. Shim, K. Kudo, M. Asada, and S. Arai, "Band gap shrinkage in GaInAs/GaInAsP/InP multi-quantum well lasers," *J. Appl. Phys.*, vol. 72, pp. 279–281, July 1992.

[28] R. O. Miles, M. A. Dupertuis, F. K. Reinhart, and P. M. Brosson, "Gain measurements in InGaAs/InGaAsP multiquantum-well broad-area lasers," *Proc. Inst. Elect. Eng.* vol. 139, pt. J, pp. 33–38, Feb. 1992.

[29] N. Suzuki and M. Ishikawa, "A small-signal frequency response model with electron and hole transport in multiquantum-well lasers," *IEEE Photon. Technol. Lett.*, vol. 5, pp. 767–770, July 1993.

[30] M. Asada, "Intraband relaxation time in quantum-well lasers," *IEEE J. Quantum Electron.*, vol. 25, pp. 2019–2026, Sept. 1989.

[31] A. Uskov, J. Mork, and J. Mark, "Wave mixing in semiconductor laser amplifier due to carrier heating and spectral-hole burning," *IEEE J. Quantum Electron.*, vol. 30, pp. 1769–1781, Aug. 1994.

[32] C. Y. Tsai, R. M. Spencer, Y. H. Lo, and L. F. Eastman, "Nonlinear gain coefficient in semiconductor lasers: Effects of carrier heating," *IEEE J. Quantum Electron.*, vol. 32, pp. 201–212, Feb. 1996.

[33] D. Bimberg and J. Mycielski, "Recombination induced heating of free carriers in a semiconductor," *Phys. Rev. B*, vol. 31, pp. 5490–5493, Apr. 1985.

[34] J. M. Luttinger and W. Kohn, "Motion of electrons and holes in perturbed periodic field," *Phys. Rev.*, vol. 97, pp. 869–883, 1955.
[35] G. E. Pikus and G. L. Bir, "Effects of deformation on the hole energy spectrum of germanium and silicon," *Sov. Phys. Solid State*, vol. 1, pp. 1502–1517, 1960.
[36] D. Ahn and S. L. Chuang, "Optical gain in a strained-layer quantum-well laser," *IEEE J. Quantum Electron.*, vol. 24, pp. 2400–2406, Dec. 1988.
[37] M. Sargent, III, M. O. Scully, and W. E. Lamb, Jr., *Laser Physics.* Reading, MA: Addison-Wesley, 1974.
[38] N. Ogasawara and R. Ito, "Longitudinal mode competition and asymmetric gain saturation in semiconductor injection lasers. II: Theory," *Jpn. J. Appl. Phys.*, vol. 27, pp. 615–626, Apr. 1988.
[39] M. Asada, A. Kameyama, and Y. Suematsu, "Gain and intervalence band absorption in quantum-well lasers," *IEEE J. Quantum Electron.*, vol. QE-20, pp. 745–753, July 1984.
[40] M. Asada and Y. Suematsu, "Density matrix theory of semiconductor lasers with relaxation broadening model-gain and gain suppression in semiconductor lasers," *IEEE J. Quantum Electron.*, vol. QE-21, pp. 434–442, May 1985.
[41] J. D. Park, D. S. Seo, and J. G. McInerney, "Self-pulsations in strongly coupled asymmetric external cavity semiconductor lasers," *IEEE J. Quantum Electron.*, vol. 26, pp. 1353–1362, Aug. 1990.
[42] H. Rong-Qing and T. Shang-Ping, "Improved rate equations for external cavity semiconductor lasers," *IEEE J. Quantum Electron.*, vol. 25, pp. 1580–1584, June 1989.
[43] P. A. Morton, V. Mizrahi, T. Tanbun-Ek, R. A. Logan, P. J. Lemaire, H. M. Presby, T. Erdogan, S. L. Woodward, J. E. Sipe, M. R. Phillips, A. M. Sergent, and K. W. Wecht, "Stable single mode hybrid laser with high power and narrow linewidth," *Appl. Phys. Lett.*, vol. 64, pp. 2634–2636, May 1994.
[44] Z. Ahmed, "Dynamics of actively mode-locked semiconductor lasers," Ph.D. dissertation, Univ. of Melbourne, Australia, Aug. 1994.
[45] C. R. Doerr, M. Zirngibl, and C. H. Joyner, "Single longitudinal mode stability via wave mixing in long-cavity semiconductor lasers," *IEEE Photon. Technol. Lett.*, vol. 7, pp. 1267–1269, Sept. 1995.
[46] P. S. Zory, Jr., Ed., *Quantum Well Lasers.* Boston, MA: Academic, 1993.
[47] R. Nagarajan and J. E. Bowers, "Effects of carrier transport on injection efficiency and wavelength chirping in quantum-well lasers," *IEEE J. Quantum Electron.*, vol. 29, pp. 1601–1608, June 1993.
[48] L. Poladian, "Variational technique for nonuniform grating and distributed-feedback lasers," *J. Opt. Soc. Amer. A*, vol. 11, pp. 1846–1853, June 1994.
[49] H. Kogelnik and C. V. Shank, "Coupled-wave theory of distributed feedback lasers," *J. Appl. Phys.*, vol. 43, pp. 2327–2335, 1972.
[50] T. A. DeTemple and C. M. Herzinger, "On the semiconductor laser logarithmic gain-current density relation," *IEEE J. Quantum Electron.*, vol. 29, pp. 1246–1252, May 1993.
[51] M. Asada, A. Kameyama, and Y. Suematsu, "Gain and intervalence band absorption in quantum-well lasers," *IEEE J. Quantum Electron.*, vol. QE-20, pp. 745–753, July 1984.
[52] C. S. Chang and S. L. Chuang, "Modeling of strained quantum-well lasers with spin-orbit coupling," *IEEE J. Select. Topics Quantum Electron.*, vol. 1, pp. 218–229, June 1995.
[53] E. P. O'Reilly and A. R. Adams, "Band-structure engineering in strained semiconductor lasers," *IEEE J. Quantum Electron.*, vol. 30, pp. 366–379, Feb. 1994.
[54] D. Ahn and S. L. Chuang, "The theory of strained-layer quantum well lasers with bandgap renormalization," *IEEE J. Quantum Electron.*, vol. 30, Feb. 1994.
[55] T. Makino, "Analytical formulas for the optical gain of quantum wells," *IEEE J. Quantum Electron.*, vol. 32, pp. 493–501, Mar. 1996.
[56] D. Kasemset, C. S. Hong, N. B. Patel, and P. D. Dapkus, "Graded barrier single quantum well lasers—Theory and experiment," *IEEE J. Quantum Electron.*, vol. QE-19, pp. 1025–1030, 1983.
[57] R. F. S. Riberio, J. R. F. da Rocha, A. V. T. Cartaxo, H. J. A. da Silva, B. Franz, and B. Wedding, "FM response of quantum-well lasers taking into account carrier transport effects," *IEEE Photon. Technol. Lett.*, vol. 7, pp. 857–859, Aug. 1995.
[58] M. Yamada and Y. Haraguchi, "Linewidth broadening of SCH quantum-well lasers enhanced by carrier fluctuation in optical guiding layers," *IEEE J. Quantum Electron.*, vol. 27, pp. 1676–1681, June 1991.
[59] M. Yamada and K. Omi, "Optimum structure of a potential controlled low threshold laser," *Trans. IEICE Japan*, vol. E71, no. 6, pp. 607–613, 1988.
[60] K. Uomi, T. Mishima, and N. Chinone, "Modulation-doped multi quantum well (MD-MQW) lasers—II. Experiment," *Jpn. J. Appl. Phys.*, vol. 29, pp. 88–94, 1990.

Malin Premaratne (S'95), photograph and biography not available at the time of publication.

Arthur J. Lowery (M'92–SM'96), photograph and biography not available at the time of publication.